



Article

# Characterization of Imidazole Compounds in Aqueous Secondary Organic Aerosol Generated from Evaporation of Droplets Containing Pyruvaldehyde and Inorganic Ammonium

Xin Lin <sup>1</sup>, Mingqiang Huang <sup>1,\*</sup> , Tingting Lu <sup>1</sup>, Weixiong Zhao <sup>2</sup>, Changjin Hu <sup>2</sup>, Xuejun Gu <sup>2</sup> and Weijun Zhang <sup>2,\*</sup>

- <sup>1</sup> Fujian Province Key Laboratory of Modern Analytical Science and Separation Technology, College of Chemistry & Chemical Engineering and Environment, Minnan Normal University, Zhangzhou 363000, China; linxin01c28@163.com (X.L.); lutingt215@163.com (T.L.)
- <sup>2</sup> Laboratory of Atmospheric Physico-Chemistry, Anhui Institute of Optics and Fine Mechanics, Chinese Academy of Sciences, Hefei 230031, China; wxzhaoaifm@gmail.com (W.Z.); hucjaiofm@gmail.com (C.H.); xjguiaofm@gmail.com (X.G.)
- \* Correspondence: huangmingqiang@mnnu.edu.cn (M.H.); wjzhangaoifm@gmail.com (W.Z.); Tel.: +86-596-2591-445 (M.H.); Fax: +86-596-2026-037 (M.H.)



**Citation:** Lin, X.; Huang, M.; Lu, T.; Zhao, W.; Hu, C.; Gu, X.; Zhang, W. Characterization of Imidazole Compounds in Aqueous Secondary Organic Aerosol Generated from Evaporation of Droplets Containing Pyruvaldehyde and Inorganic Ammonium. *Atmosphere* **2022**, *13*, 970. <https://doi.org/10.3390/atmos13060970>

Academic Editors: Xiao Sui and Houfeng Liu

Received: 3 May 2022

Accepted: 13 June 2022

Published: 15 June 2022

**Publisher's Note:** MDPI stays neutral with regard to jurisdictional claims in published maps and institutional affiliations.



**Copyright:** © 2022 by the authors. Licensee MDPI, Basel, Switzerland. This article is an open access article distributed under the terms and conditions of the Creative Commons Attribution (CC BY) license (<https://creativecommons.org/licenses/by/4.0/>).

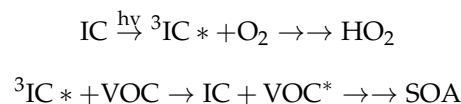
**Abstract:** Imidazole compounds are important constituents of atmospheric brown carbon. The imidazole components of aqueous secondary organic aerosol (aqSOA) that are generated from the evaporation of droplets containing pyruvaldehyde and inorganic ammonium are on-line characterized by an aerosol laser time-of-flight mass spectrometer (ALTOFMS) and off-line detected by optical spectrometry in this study. The results demonstrated that the laser desorption/ionization mass spectra of aqSOA particles that were detected by ALTOFMS contained the characteristic mass peaks of imidazoles at  $m/z = 28$  ( $\text{CH}_2\text{N}^+$ ),  $m/z = 41$  ( $\text{C}_2\text{H}_3\text{N}^+$ ) and  $m/z = 67$  ( $\text{C}_3\text{H}_4\text{N}_2^+$ ). Meanwhile, the extraction solution of the aqSOA particles that were measured by off-line techniques showed that the characteristic absorption peaks at 217 nm and 282 nm appeared in the UV-Vis spectrum, and the stretching vibration peaks of C-N bond and C=N bond emerged in the infrared spectrum. Based on these spectral information, 4-methyl-imidazole and 4-methyl-imidazole-2-carboxaldehyde are identified as the main products of the reaction between pyruvaldehyde and ammonium ions. The water evaporation accelerates the formation of imidazoles inside the droplets, possibly owing to the highly concentrated environment. Anions, such as  $\text{F}^-$ ,  $\text{CO}_3^{2-}$ ,  $\text{NO}_3^-$ ,  $\text{SO}_4^{2-}$  and  $\text{Cl}^-$  in the aqueous phase promote the reaction of pyruvaldehyde and ammonium ions to produce imidazole products, resulting in the averaged mass absorption coefficient ( $\langle \text{MAC} \rangle$ ) in the range of 200–600 nm of aqSOA increases, and the order of promotion is:  $\text{F}^- > \text{CO}_3^{2-} > \text{SO}_4^{2-} \approx \text{NO}_3^- \approx \text{Cl}^-$ . These results will help to analyze the constituents and optics of imidazoles and provide a useful basis for evaluating the formation process and radiative forcing of aqSOA particles.

**Keywords:** pyruvaldehyde; inorganic ammonium; aqueous secondary organic aerosol; imidazole compounds; brown carbon

## 1. Introduction

Organic carbon (OC) is a vital component of atmospheric aerosol particles. OC that can absorb light in the ultraviolet-near visible range (300–400 nm) and has wavelength-dependent light absorption properties is called brown carbon (BrC) [1,2]. BrC can absorb and scatter solar radiation, leading to the reduction in atmospheric visibility, and it has gradually become an important driving factor affecting radiative forcing and disturbing regional climate change [3,4]. Imidazoles, such as imidazole and imidazole-2-carboxaldehyde have certain toxicity, are irritating and corrosive to skin and mucous membranes, and endanger human health [5]. Imidazoles also contain the chromophores of C=N and C=C,

which are important brown carbon components [1,6,7]. In addition, imidazolaldehydes are the common photosensitizers in the atmosphere. For example, imidazole-2-carboxaldehyde (IC) absorbs ultraviolet radiation and forms the triplet excited state of IC ( $^3\text{IC}^*$ ) [8,9], which can either reduce  $\text{O}_2$  to form  $\text{HO}_2$  radicals and other oxidizing radicals [10,11] or interact with other volatile organic compound (VOC) as follows:



${}^3\text{IC}^*$  oxidizes other VOC (also called substrate) via energy transfer, electron transfer or H- abstraction. While the substrate is transformed, the photosensitizer can either be degraded or possibly regenerated, resulting in a photocatalytic process and the generation of secondary organic aerosol (SOA) particles [12,13]. Therefore, the formation process and optical properties of imidazoles have attracted extensive attention.

Except for the primary emission source of combustion, the aqueous reaction of glyoxal, pyruvaldehyde and other  $\alpha$ -dicarbonyl compounds with ammonium sulphate is an important secondary source of imidazole compounds. Glyoxal and pyruvaldehyde are mainly derived from the direct emission of biomass combustion [14] and the oxidation of VOCs that are emitted from biological sources (isoprene, terpene, etc.) [15] and anthropogenic sources (acetylene, aromatic compounds, etc.) [16,17]. The annual global glyoxal emission is estimated to be about 45 Tg, of which 47% is produced by the photooxidation of isoprene and 20% from biomass combustion [18,19]. Meanwhile, pyruvaldehyde is widely present in urban, rural and remote environments, with an annual emission of 140 Tg, 79% from isoprene oxidation, and acetone oxidation is its second largest source [19]. Glyoxal and methylglyoxal have high Henry coefficients ( $10^3$ – $10^5$  M/atm) in the aqueous phase and can be transferred to liquid aerosol particles, water droplets and clouds through gas/liquid partitioning [20]. Nozière et al. [21] observed that there were UV absorption peaks in the aqueous products of  $(\text{NH}_4)_2\text{SO}_4$  and glyoxal, and their reaction rate constants increased with the increase in  $\text{NH}_4^+$  activity and pH of aqueous solution. They propose that the nitrogen-containing organic products were formed from an imine path under the action of  $\text{NH}_4^+$  to glyoxal. Kampf et al. [22] conducted the optical and mass spectra measurements on the aqueous reaction products of glyoxal and  $(\text{NH}_4)_2\text{SO}_4$  and found that the products had an absorption peak at 280 nm, and imidazole, imidazole-2-carboxaldehyde and 2,2'-bis-imidazole were the main aqueous reaction products. Lee et al. [23] further confirmed that the SOA particles formed by the evaporation of water droplets comprising glyoxal and  $(\text{NH}_4)_2\text{SO}_4$  contained imidazole and imidazole-2-carboxaldehyde. Maxut et al. [24] detected imidazole, imidazole-2-carboxaldehyde, 2,2'-bis-imidazole and other imidazoles that are formed from the reaction of glyoxal and  $(\text{NH}_4)_2\text{SO}_4$  under neutral conditions (pH = 7). Further, Teich et al. [25,26] isolated and identified imidazoles, such as 4(5)-methyl-imidazole, imidazol-2-carboxaldehyde and ethyl-imidazole in atmospheric aerosol samples from Germany, Italy and China, and measured their concentrations between 0.2 and 14 ng/m<sup>3</sup>. Lian et al. [27] detected that 60% of imidazoles were mixed with carbonyl and ammonium/amine inside the particles, confirming the reaction of carbonyl and ammonium/amine at the single particle level to form imidazoles.

However, the above experiments mainly focus on the identification of the aqueous reaction products of glyoxal and  $(\text{NH}_4)_2\text{SO}_4$  via off-line methods [21–24]. Moreover, Powellson et al. [28] measured the absorption Ångstrom coefficients ( $\text{\AA}_{\text{abs}}$ ) of the reaction product solution of glyoxal and other carbonyl compounds with  $(\text{NH}_4)_2\text{SO}_4$  to be between 2 and 11, which falls within the range of the  $\text{\AA}_{\text{abs}}$  of atmospheric water-soluble brown carbon. Further, the complex refractive index (CRI) and mass absorption coefficient (MAC) of the aqSOA particles that are produced by the reaction of methylglyoxal and  $(\text{NH}_4)_2\text{SO}_4$  are detected by Tang et al. [29] and Harrison et al. [30]. The obtained real part (n) of the CRI at 402 nm is between 1.46 and 1.52, and the imaginary part (k) is less than 0.01 [29]. The measured MAC value at 280 nm is about 1330 cm<sup>2</sup>/g [30]. Although these experiments

measured optical parameters, such as the CRI and MAC of aqSOA particles, the influence of other components in aqueous phase are not considered. In addition to  $\text{NH}_4^+$  ions, anions such as  $\text{NO}_3^-$ ,  $\text{SO}_4^{2-}$ ,  $\text{CO}_3^{2-}$ ,  $\text{Cl}^-$  and  $\text{F}^-$  are also in the aqueous phase [31–33].  $\text{NO}_3^-$  and  $\text{SO}_4^{2-}$  ions that are mainly formed by the atmospheric chemical conversion of  $\text{NO}_x$  and  $\text{SO}_2$  emitted from the combustion of coal, petroleum and other chemical fuels are important components of  $\text{PM}_{2.5}$  particles [34].  $\text{Cl}^-$  and  $\text{F}^-$  ions mostly come from sea salt aerosol [35], while  $\text{CO}_3^{2-}$  ion primarily originates from mineral dust [36]. However, the effects of these anions on the formation and optics of imidazole compounds have not been reported. As the annual global pyruvaldehyde emission is greater than that of glyoxal [19], it widely exists in atmospheric aqueous phase and is an important contributor to the potential formation of SOA and imidazole compounds. Therefore, pyruvaldehyde is selected as the precursor of imidazoles in this study. The solutions of pyruvaldehyde and inorganic ammonium are atomized by TSI 9302, and the aqSOA particles are obtained after drying through a silica gel diffusion tube. Imidazole components are measured by on-line and off-line mass and optical spectrometry to study their formation mechanism. In addition, a UV-Vis spectrophotometer and total organic carbon analyzer (TOC) are combined to measure the mass absorption coefficient (MAC) to quantitatively characterize the light absorption of aqSOA particles. The effects of different water-soluble anions, such as  $\text{NO}_3^-$ ,  $\text{SO}_4^{2-}$ ,  $\text{CO}_3^{2-}$ ,  $\text{Cl}^-$  and  $\text{F}^-$  on the MAC of aqSOA produced by the reaction of pyruvaldehyde and inorganic ammonium salts are investigated. These provide a useful basis for the study of the formation and optical properties of imidazole compounds in atmospheric aqSOA particles.

## 2. Experiments

### 2.1. Material

Pyruvaldehyde (40% solution); methanol (>99%); imidazole ( $\geq 99.5\%$ ); 4-methyl-imidazole ( $\geq 98\%$ ); imidazole-2-carboxaldehyde ( $\geq 99.0\%$ ); and 4-methyl-imidazole-2-carboxaldehyde (99%) are obtained from Aladdin reagent Shanghai Co., Ltd. (Shanghai, China). Ammonium sulfate ( $\geq 99.0\%$ ); ammonium chloride ( $\geq 99.5\%$ ); ammonium nitrate ( $\geq 99.0\%$ ); ammonium fluoride ( $\geq 96.0\%$ ); and ammonium carbonate ( $\geq 96.0\%$ ) are purchased from Sigma Aldrich Shanghai Trading Co., Ltd (Shanghai, China). These materials are not further purified and directly used in the experiments.

### 2.2. Formation of aqSOA by the Evaporation of Droplets Containing Pyruvaldehyde with $(\text{NH}_4)_2\text{SO}_4$

Researchers often prepare a certain concentration solution according to the concentration of organic and inorganic substances in the atmospheric aqueous phase, and then evaporate water to simulate the generation of aqSOA particles. The solution is generally atomized by a commercial atomizer (TSI 3076 or TSI 9302) to generate liquid aerosol particles, and then the water is evaporated through a silica gel diffusion tube to form the aqSOA particles [23,37]. Some researchers have also removed the water by rotary evaporation of the solution at a certain temperature to obtain aqSOA particles [38]. The latter is the evaporation of water in the solution under the condition of a relatively high temperature and rotational vibration, which can quickly complete the aqueous reaction and evaporation of water but cannot adequately simulate the actual atmospheric aqueous reaction process. Therefore, the former method is adopted in this study. A total of 3.303 g ammonium sulfate is dissolved by deionized water and transferred to a 250 mL volumetric flask; 2 mL of 40% pyruvaldehyde solution is added to the flask and the mixed solution of 5 mmol/L of pyruvaldehyde and 10 mmol/L of ammonium sulfate is obtained after constant volume by deionized water. Then, the mixed solution is transferred to a TSI 9302 atomizer. As shown in Figure 1, the mixed solution is atomized at a pressure of  $0.83 \times 10^5$  Pa to generate aerosol particles with a particle size ranging from 0.1 to 2  $\mu\text{m}$ . After drying through a silica gel diffusion tube, aqSOA particles with the concentration of about 200  $\mu\text{g}/\text{m}^3$  are

achieved. The aqSOA particles are detected on-line by an aerosol laser time-of-flight mass spectrometer (ALTOFMS) [39,40].

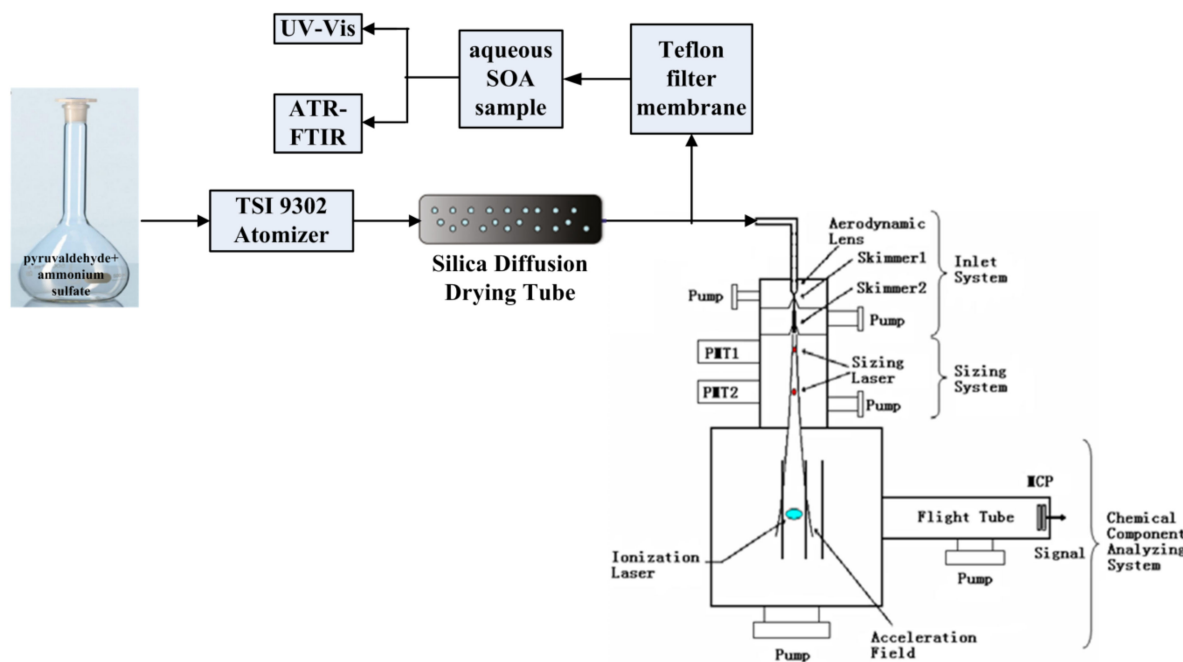


**Figure 1.** Schematic diagram for the characterization of aqSOA produced by the evaporation of droplets containing pyruvaldehyde and  $(\text{NH}_4)_2\text{SO}_4$ .

Owing to the volatility of pure methanol, 2% methanol water solution is used to extract the organic components of the aqSOA particles, which has a good extraction effect, and the extract solution can be utilized for the detection with UV-Vis in our previous studies [41,42]. Thus, the aqSOA particles are collected by a Teflon filter membrane and extracted into 5 mL of 2% methanol water solution by sonicating for 30 min. In order to eliminate the measurement error, the aqSOA particles are extracted immediately after collection. The Teflon filter membrane is placed in a small beaker containing 5 mL of 2% methanol water solution and covered with a glass-surface vessel to prevent the loss of solvent volatilization during the 30-min ultrasonic extraction. A secondary extraction is also performed to confirm that the primary extraction is complete when the absorption spectrum of its extraction is approximately a straight line. Each experiment is performed three times in parallel and the averaged value is taken as the final analysis data for off-line measurement.

### 2.3. Characterization of Imidazole Products in aqSOA

The ALTOFMS is used to detect aqSOA particles in real-time [39,40]. As shown in Figure 1, the aqSOA particles that are formed from the evaporation of droplets containing pyruvaldehyde and  $(\text{NH}_4)_2\text{SO}_4$  are entered into the aerodynamic lens and two skimmers to form a collimated particle beam, which is introduced into the sizing system. The particle size is obtained by measuring the transit time of the particle through two 532 nm lasers in sequence. Then, the particle is transferred to the vacuum ionization chamber, desorbed and ionized by a 266 nm Nd:YAG pulsed laser with a density of  $10^7 \text{ W/cm}^2$ . The generated ions are accelerated into the time-of-flight mass spectrometer, detected by the dual microchannel plate detector, and the complete ion mass spectrum of aqSOA particle is obtained [39,40]. A UV-Vis spectrophotometer (UV-6100S, Mapada Instruments, Shanghai, China) and attenuated total reflection Fourier transformed infrared spectroscopy (ATR-FTIR, Thermo Nicolet iS 10, Thermo Fisher Scientific, Waltham, MA, USA) are also used for off-line measurement to verify the imidazole products in the extraction of aqSOA.

#### 2.4. Optical Characterization of aqSOA

Updyke et al. [43] and Powelson et al. [28] have utilized Equations (1) and (2) to calculate the mass absorption coefficient (MAC) ( $\text{cm}^2/\text{g}$ ) to quantify the effect of organic aerosols on light absorption.

$$\text{MAC}(\lambda) = \frac{A^{\text{solution}}(\lambda) \times \ln 10}{b \times C_{\text{mass}}} \quad (1)$$

$$\langle \text{MAC} \rangle = \frac{1}{(\lambda_2 - \lambda_1)} \times \int_{\lambda_1}^{\lambda_2} \text{MAC}(\lambda) d\lambda \quad (2)$$

In Equation (1),  $A^{\text{solution}}$  is the absorbance of the extraction solution of aqSOA particles at  $\lambda$ ,  $b$  is the optical path length (i.e., the cuvette width, cm), and  $C_{\text{mass}}$  is the organic carbon concentration of the extraction solution ( $\text{g}/\text{cm}^3$ ). According to equation (2), the averaged MAC ( $\langle \text{MAC} \rangle$ ) is acquired by integrating in the range of  $\lambda_1$ – $\lambda_2$ .

A total of 5 mmol/L of pyruvaldehyde is kept unchanged; the mixed solution of pyruvaldehyde and 20 mmol/L of ammonium ions (10 mmol/L of  $(\text{NH}_4)_2\text{SO}_4$  and  $(\text{NH}_4)_2\text{CO}_3$ , and 20 mmol/L of  $\text{NH}_4\text{F}$ ,  $\text{NH}_4\text{NO}_3$  and  $\text{NH}_4\text{Cl}$ ) is prepared successively. The extraction solutions of the aqSOA particles that are produced by the reaction of pyruvaldehyde with inorganic ammonium salts are obtained according to the method in 2.2. The UV-Vis spectrophotometer is used to measure the absorption spectrum of the extraction solution in 200–600 nm with the 2% methanol water solution as a reference and a quartz cuvette with a width of 1 cm, combined with the organic carbon analyzer (TOC-L, Shimadzu Company, Kyoto, Japan) to measure the total organic carbon concentration of the extraction solution. The sample and high-purity  $\text{O}_2$  are introduced into the high-temperature combustion tube and low-temperature reaction tube of TOC-L. The sample through the high-temperature combustion tube is oxidized at a high temperature, and the organic and inorganic carbonate components are decomposed into  $\text{CO}_2$ . Meanwhile, the sample in the low-temperature reaction tube is acidified by phosphoric acid and the inorganic carbonate components are transformed into  $\text{CO}_2$ . The generated  $\text{CO}_2$  is successively introduced into the non-dispersive infrared detector to obtain the peak signal. The measured peak area value is the integral value of the  $\text{CO}_2$  absorption rate and time, and the difference between the concentration of total carbon and inorganic carbon is the total concentration of organic carbon [44]. The organic carbon concentration ( $C_{\text{mass}}$ ) of the extract solution is obtained by subtracting the organic carbon concentration of the 2% methanol water solution from the total organic carbon concentration that is measured. The  $\langle \text{MAC} \rangle$  that averaged over 200–600 nm of aqSOA is calculated according to Formulas (1) and (2).

### 3. Results

#### 3.1. On-Line Characterization of Imidazole Products

The off-line analysis method's sample preparation procedure is cumbersome and time-consuming, so it cannot provide component information quickly. Based on this, this study carries out on-line detection research with the help of ALTOFMS [39,40]. In order to confirm whether the ALTOFMS can be used for the detection of imidazole compounds, the laser desorption/ionization of imidazole compounds are carried out first. A total of 100 mL of 0.1 mmol/L imidazole, 4-methyl-imidazole, imidazole-2-carboxaldehyde and 4-methyl-imidazole-2-carboxaldehyde solution is successively transferred to TSI 9302. After atomization and drying, the SOA particles are generated and entered into ALTOFMS for detection. The generated positive ions are measured by time-of-flight mass spectrometry to acquire the positive-ion mass spectrum of a single particle. According to the design principles of ALTOFMS, the laser desorption/ionization mass spectrum of a single particle is only obtained once its diameter has been measured [39,40]. A total of 200 single aerosol particles' mass spectra are collected for each sample, and the averaged mass spectra of all particles are taken as the mass spectrum of the substance. The averaged laser desorption/ionization positive-ion mass spectra of imidazole, 4-methyl-imidazole, imidazole-2-carboxaldehyde

and 4-methyl-imidazole-2- carboxaldehyde particles are shown in Figures 2 and 3, respectively.

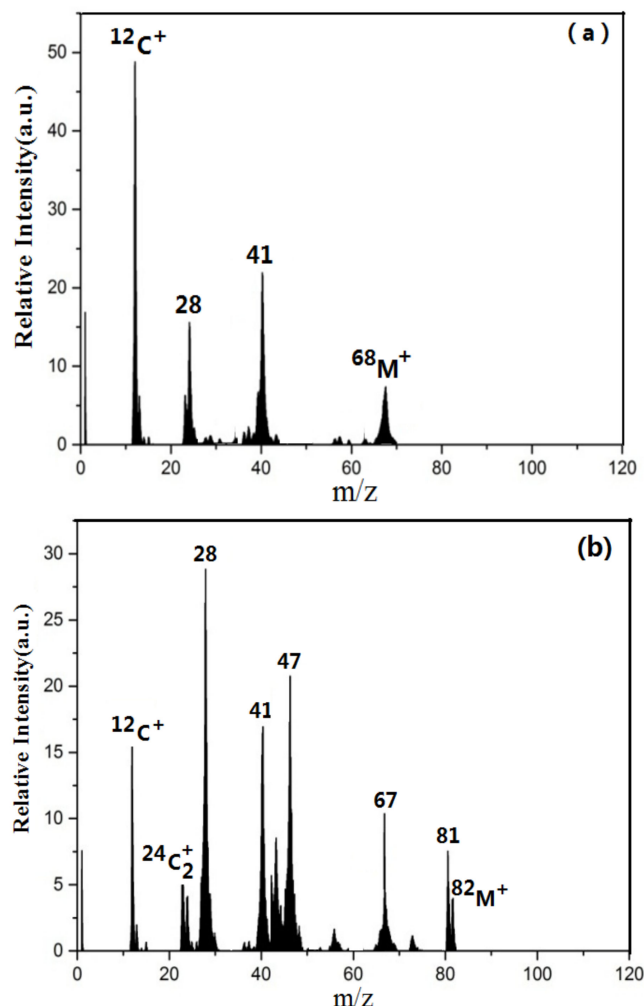


**Figure 2.** The averaged laser desorption/ionization positive-ion mass spectrum of (a) imidazole and (b) 4-methyl-imidazole particles.

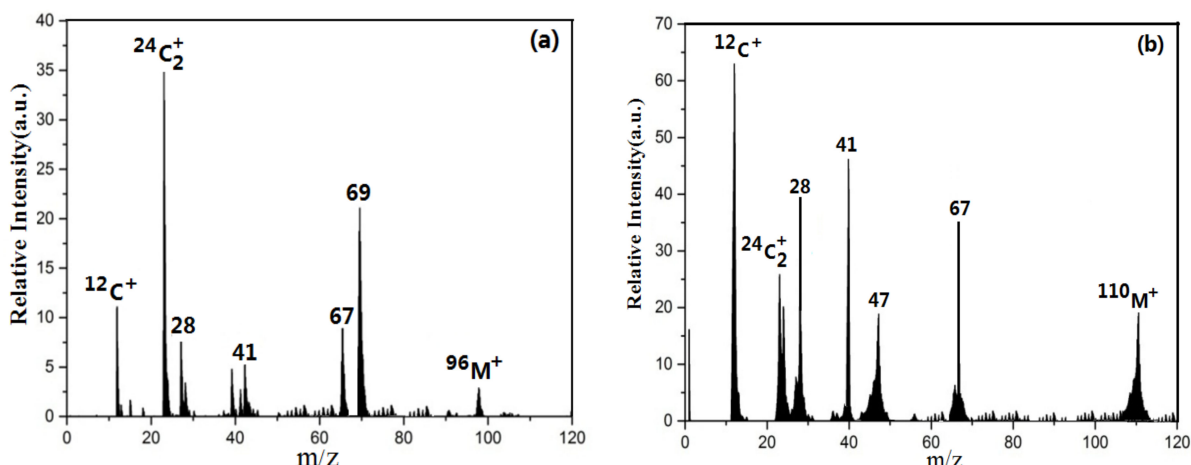


**Figure 3.** The averaged laser desorption/ionization positive-ion mass spectrum of (a) imidazole-2-carboxaldehyde and (b) 4-methyl-imidazole-2-carboxaldehyde particles.

There are mass peaks with  $m/z$  of 12, 28, 41 and 68 in the average positive-ion mass spectrum of imidazole particles as displayed in Figure 2a, among which  $m/z = 12$  is the  $C^+$  ion mass peak that is generated by the cracking of an organic compound [45]. Imidazole is a five-membered ring structure containing nitrogen atoms, which is relatively stable. With a mass peak at  $m/z$  of 68, its mass-charge-ratio is the same as the molecular weight (Mw) of imidazole, corresponding to the molecular ion peak of imidazole ( $M^+, C_3H_4N_2^+$ ) [23,46]. As suggested by Lee et al. [23] and Liu et al. [46], the molecular ion of imidazole may be fragmented to generate characteristic ions of  $C_2H_3N^+$  ( $m/z = 41$ ) and  $CH_2N^+$  ( $m/z = 28$ ). The averaged positive ion-mass spectrum of 4-methyl-imidazole particles illustrated in Figure 2b obviously has imidazole characteristic ion peaks with  $m/z = 67$  ( $C_3H_3N_2^+$ ),  $m/z = 41$  ( $C_2H_3N^+$ ) and  $m/z = 28$  ( $CH_2N^+$ ) [23,46]. In addition, there is an obvious mass peak at  $m/z = 82$  in Figure 2b, which is considered to be the molecular ion peak of 4-methyl-imidazole ( $M^+, C_4H_6N_2^+$ ) as the mass-to-charge ratio is the same as its molecular weight. The mass peaks of  $m/z = 81$  may correspond to the ion peaks of one methyl group on the imidazole ring ( $(C_3H_2N_2 + CH_3)^+$ ), which is generated by the loss of a hydrogen atom in the molecular ion peak of 4-methyl-imidazole [47].

Similarly, the averaged positive-ion mass spectrum of imidazole-2-carboxaldehyde and 4- methyl-imidazole-2-carboxaldehyde particles illustrated in Figure 3 obviously has imidazole characteristic ion peaks with  $m/z = 67$  ( $C_3H_3N_2^+$ ),  $m/z = 41$  ( $C_2H_3N^+$ ) and  $m/z = 28$  ( $CH_2N^+$ ) [23,46]. In addition, the obvious mass peak at  $m/z = 96$  and  $m/z = 110$  is presented in Figure 3a,b, respectively, which is considered to be the molecular ion peak of imidazole-2-carbaldehyde ( $M^+, C_4H_4N_2O^+$ ) and 4-methyl-imidazole-2-carboxaldehyde ( $M^+, C_5H_6N_2O^+$ ) as the mass-to-charge ratio is the same as its molecular weight, respectively [47]. Compared with the electron bombardment mass spectra of imidazole and imidazole-2-carbaldehyde that were obtained by Lee et al. [23], the characteristic mass spectra are still similar despite the different ionization methods that are used. This indicates that ALTOFMS with laser desorption/ionization can be used for the on-line measurement of imidazoles.

Based on the obtained mass spectra of imidazole compounds, the on-line measurement of aqSOA particles that are formed from the evaporation of droplets containing pyruvaldehyde and  $(NH_4)_2SO_4$  is subsequently carried out. The averaged positive-ion mass spectrum of 200 aqSOA particles is illustrated in Figure 4. Since the aqSOA contains multiple components, the mass spectrum is complex, but still clearly shows the characteristic mass peaks of imidazoles at  $m/z = 28$  ( $CH_2N^+$ ),  $m/z = 41$  ( $C_2H_3N^+$ ) and  $m/z = 67$  ( $C_3H_3N_2^+$ ) [23,46], indicating that the reaction of pyruvaldehyde and  $(NH_4)_2SO_4$  produces imidazole products. Except for the  $C^+$  and  $C_2^+$  fragment peak at  $m/z = 12$  and  $m/z = 24$ , the peak with  $m/z = 18$  corresponds to the  $NH_4^+$  ion peak. It may be that the unreacted  $(NH_4)_2SO_4$  is atomized, dried to form particles, and ionized by the 266 nm Nd:YAG pulsed laser to generate  $NH_4^+$  ion. On the other hand, the mass peaks with  $m/z = 47$  and 58 may correspond to the fragment ion peak of the hydration products of pyruvaldehyde [23,48]. The mass peaks of  $m/z = 81$  may correspond to the ion peaks of one methyl group on the imidazole ring ( $(C_3H_2N_2 + CH_3)^+$ ), demonstrating methyl-substituted imidazoles in the aqSOA particles. In addition, there are obvious mass peaks at  $m/z = 82$  and  $m/z = 110$ , which are speculated to be the molecular ion peaks of 4-methyl-imidazole ( $C_4H_6N_2^+$ , Mw = 82) and 4-methyl-imidazole-2-carbaldehyde ( $C_5H_6N_2O^+$ , Mw = 110), respectively, since the mass-to-charge ratio is the same as the molecular weight. To further confirm the imidazole components of the aqSOA particles, UV-Vis and ATR-FTIR measurements are subsequently carried out.

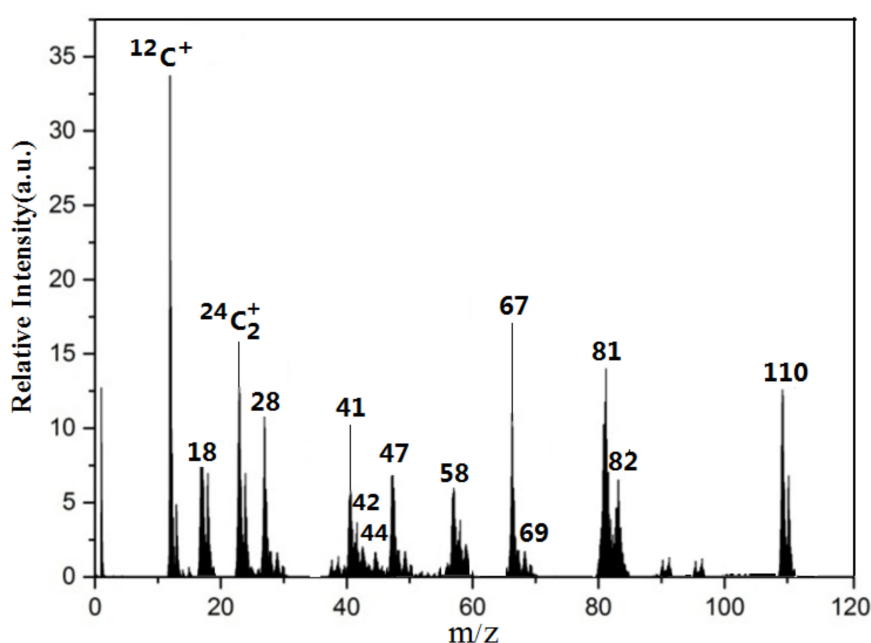


**Figure 4.** The averaged laser desorption/ionization positive-ion mass spectrum of aqSOA particles formed from the evaporation of droplets containing pyruvaldehyde and  $(\text{NH}_4)_2\text{SO}_4$ .

### 3.2. Off-Line Characterization of Imidazole Products

A total of 5 mmol/L of pyruvaldehyde and the mixed solution of 5 mmol/L of pyruvaldehyde and 10 mmol/L of  $(\text{NH}_4)_2\text{SO}_4$  is atomized and dried to produce aqSOA particles, respectively. Taking 2% methanol water solution as a reference, the absorption spectra of the extraction solutions in 200–600 nm are illustrated in Figure 5. The extraction solution of the aqSOA particles that is produced by 5 mmol/L of pyruvaldehyde is colorless and transparent, and there is a weak peak at 292 nm which corresponds to the characteristic absorption peak of carbonyl [49]. However, the extraction solution of the aqSOA particles that are formed from the mixed solution of 5 mmol/L of pyruvaldehyde and 10 mmol/L of  $(\text{NH}_4)_2\text{SO}_4$  shows brown-yellow, and its absorption spectrum has strong absorption peaks at 217 nm and 282 nm, respectively, indicating the formation of the brown carbon products with light absorption ability. Nozière et al. [21], Kampf et al. [22], Lee et al. [23] and Maxut et al. [24] also detected these two similar absorption peaks when studying the aqueous reaction of glyoxal with  $(\text{NH}_4)_2\text{SO}_4$ . They suggest that the  $\pi \rightarrow \pi^*$  electron transition of C=N in the heterocyclic ring of imidazole and imidazole-2-carbaldehyde produces the absorption peak of 209 nm, and the  $n \rightarrow \pi^*$  electron transition of C=N is responsible for the absorption peak of 280 nm. Compared with the reaction system of glyoxal and  $(\text{NH}_4)_2\text{SO}_4$ , these two UV absorption peaks of the reaction products of pyruvaldehyde and  $(\text{NH}_4)_2\text{SO}_4$  shift by about 8 nm and 2 nm, respectively, suggesting the production of 4-methyl-imidazole and 4-methyl-imidazole-2-carbaldehyde.

In order to further determine the component information of imidazoles, the absorption spectrum of the extraction solution is compared with imidazole compounds. A certain amount of imidazole, 4-methyl-imidazole, imidazole-2-carbaldehyde and 4-methyl-imidazole-2-carbaldehyde is dissolved successively in 2% methanol water solution to prepare the standard solution with a concentration of 0.1 mmol/L. Taking 2% methanol water solution as a reference, the measured UV-Vis absorption spectrum is shown in Figure 6. Imidazole has a characteristic absorption peak near 209 nm, which is similar to the UV-Vis spectrum that was reported by Maxut et al. [24]. They used water as a solvent and measured a characteristic absorption peak at 205 nm in the imidazole aqueous solution. A 2% methanol aqueous solution is used as the solvent in this study, and its characteristic absorption peak is red-shifted to 209 nm. Compared with imidazole, the characteristic absorption peak in the UV-Vis spectrum of 4-methyl-imidazole is red-shifted to 217 nm due to the existence of methyl substituent.

Similar to the UV-Vis spectrum of imidazole-2-carbaldehyde that was measured by Maxut et al. [24], the UV-vis spectrum of imidazole-2-carbaldehyde shows a weaker absorption band at 215 nm and a maximum absorption peak at 280 nm; the latter is considered as the characteristic absorption peak of imidazole-2-carbaldehyde [9,24]. Further, the absorption peaks of 4-methyl-imidazole-2-carbaldehyde shown in Figure 6 are red-shifted to 217 nm and 282 nm due to the presence of methyl groups.

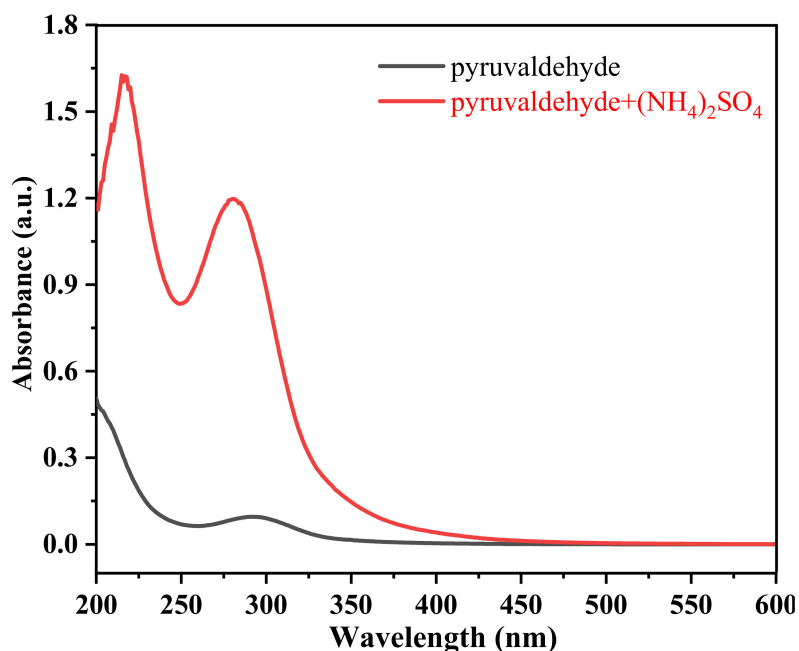


**Figure 5.** UV-Vis absorption spectra of the extraction solutions of aqSOA particles produced by 5 mmol/L pyruvaldehyde and the mixed solution of 5 mmol/L pyruvaldehyde and 10 mmol/L  $(\text{NH}_4)_2\text{SO}_4$ .

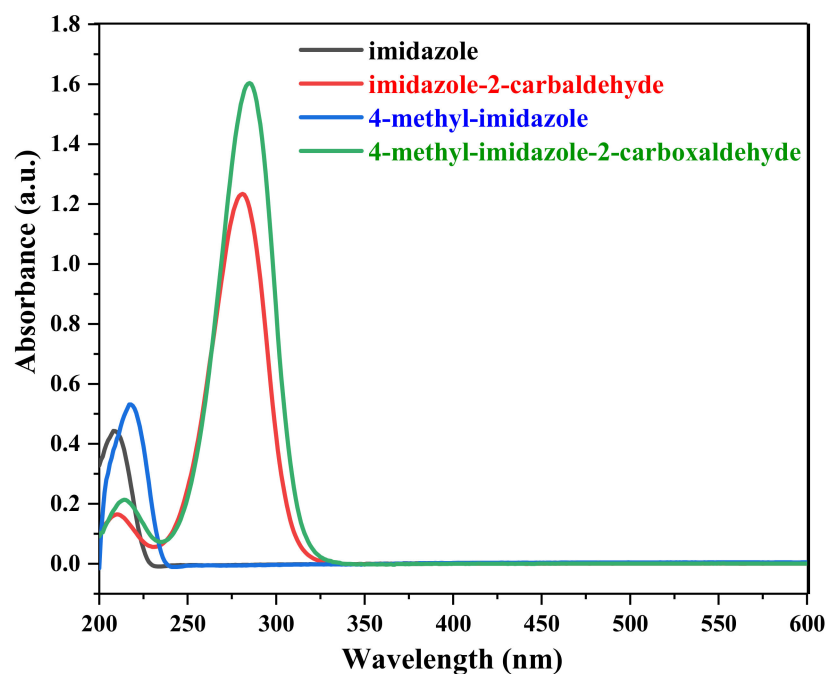


**Figure 6.** UV-Vis absorption spectra of 0.1 mmol/L imidazole, 4-methyl-imidazole, imidazole-2-carbaldehyde and 4-methyl-imidazole-2-carbaldehyde standard solutions.

To further determine the imidazole components in aqSOA particles, 5 mmol/L of pyruvaldehyde and 5, 10, 15, 20, 25 and 30 mmol/L of  $(\text{NH}_4)_2\text{SO}_4$  mixed solution is prepared and transferred to TSI 9302, atomized and dried to obtain aqSOA particles, successively. The measured UV-Vis spectra of the extraction solutions of the aqSOA particles are shown in Figure 7. It can be seen from Figure 7 that the UV-Vis spectra of the extraction solutions are basically identical, with the absorption peaks at 217 nm and 282 nm. With the increasing concentration of  $(\text{NH}_4)_2\text{SO}_4$ , the absorption peaks of the extraction solution do not shift, but the absorbance of 217 nm and 282 nm gradually increase. Combined with the UV-Vis spectra of 4-methyl-imidazole and 4-methyl-imidazole-2-carbaldehyde that are shown in Figure 6 and the on-line detection results of ALTOFMS, it can be confirmed that the main components of each extraction solution are 4-methyl-imidazole and 4-methyl-imidazole-2-carbaldehyde. As the intensity of the absorption peak at 217 nm is greater than that of 282 nm, it can be inferred that the amount of 4-methyl-imidazole is greater than that of 4-methyl-imidazole-2-carbaldehyde. It is worth noting that when the concentration of  $(\text{NH}_4)_2\text{SO}_4$  exceeds 25 mmol/L, the absorbance of the extraction solution at 217 nm and 282 nm remains almost unchanged. This is possibly because the pyruvaldehyde in the system is constant, and when the  $(\text{NH}_4)_2\text{SO}_4$  increases to 25 mmol/L, the pyruvaldehyde has been completely consumed and the produced 4-methyl-imidazole and 4-methyl-imidazole-2-carbaldehyde reach the maximum value. Upon continuing to increase the concentration of  $(\text{NH}_4)_2\text{SO}_4$ , the yield of imidazole products almost stopped increasing, and the absorbance of the extraction solution remained almost constant.

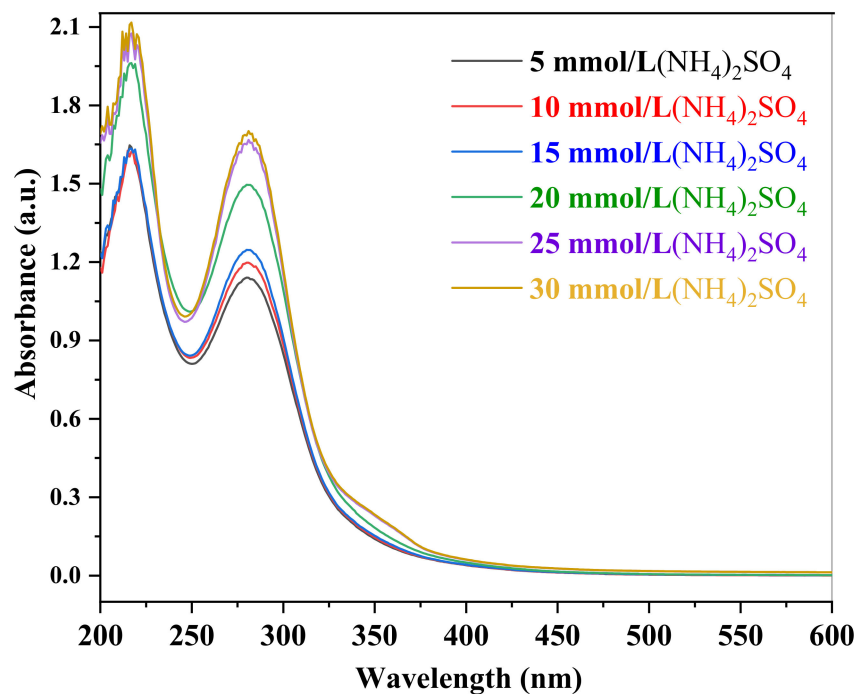


**Figure 7.** UV-Vis absorption spectra of the extraction solutions of aqSOA particles produced 5 mmol/L pyruvaldehyde and different concentrations of  $(\text{NH}_4)_2\text{SO}_4$ .

To identify imidazole products, ATR-FTIR is utilized to measure the infrared absorption spectrum of the extraction solution. During the measurement, 2% methanol water solution is used as the background, the scanning range is  $400\text{--}4000\text{ cm}^{-1}$  and the resolution is  $0.1\text{ cm}^{-1}$ . The infrared absorption spectrum of the extraction solution after subtracting the background is displayed in Figure 8. In addition to the stretching vibration of methyl's C-H near  $3000\text{ cm}^{-1}$  and the stretching vibration peak of C-O at  $1087\text{ cm}^{-1}$ , the absorption band that is generated by the stretching vibration of C-N appears at  $1453\text{ cm}^{-1}$ , and the absorption peak at  $1736\text{ cm}^{-1}$  corresponds to the stretching vibration of C=N

bond [46]. This is in good agreement with the experimental results of Liu et al. [46] and Huang et al. [50] who also detected characteristic absorption peaks near  $1450\text{ cm}^{-1}$  for the C-N bond and  $1730\text{ cm}^{-1}$  for the C=N bond when they measured the infrared spectrum of the ammonia-aged SOA particles. This further confirms that imidazoles are the main components of the aqueous SOA that is produced by the reaction of pyruvaldehyde with  $(\text{NH}_4)_2\text{SO}_4$ .

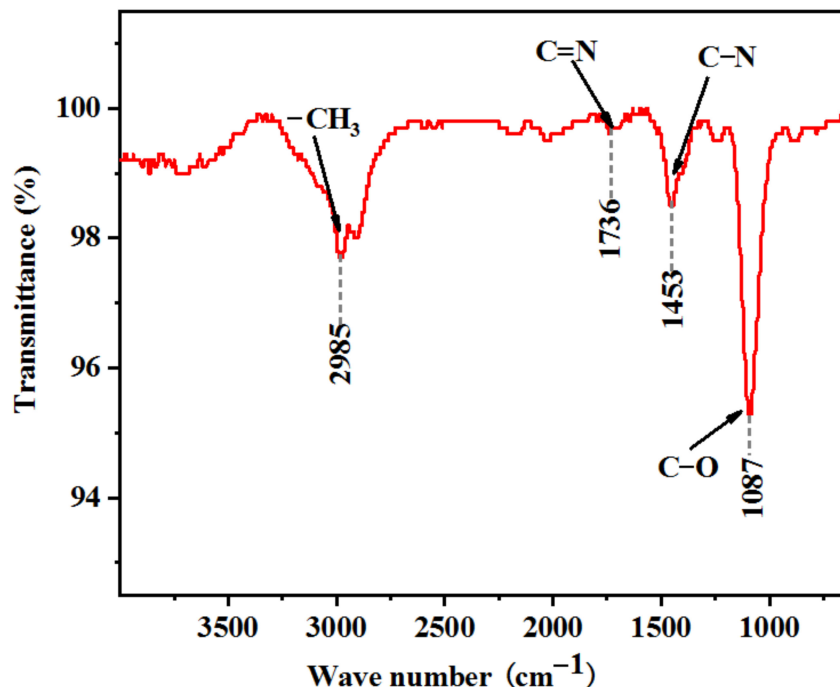


**Figure 8.** The infrared spectrum of the extraction solution of aqSOA particles produced by the mixed solution of 5 mmol/L pyruvaldehyde and 10 mmol/L  $(\text{NH}_4)_2\text{SO}_4$ .

### 3.3. Formation Mechanism of Imidazole Products

For the averaged laser desorption/ionization positive-ion mass spectrum of aqSOA particles displayed in Figure 4, in addition to the molecular ion peaks and characteristic fragment peaks of imidazole products, and the fragment ion peaks of the hydration products of pyruvaldehyde at  $m/z = 47$  and  $m/z = 58$  [48], there are  $m/z = 69$  and  $m/z = 42$  in the mass spectrum with relatively small peak intensities. According to the experimental results of Liu et al. [46], these two mass peaks may correspond to the  $\text{C}_3\text{N}_2\text{H}_5^+$  and  $\text{C}_2\text{H}_4\text{N}^+$  ion peaks. It is speculated that the methyl-diimide ( $\text{C}_3\text{N}_2\text{H}_6$  Mw = 70) molecular ion loses a hydrogen atom to generate a  $\text{C}_3\text{N}_2\text{H}_5^+$  ion, and fractures and loses  $\text{CNH}_2$  to form a  $\text{C}_2\text{H}_4\text{N}^+$  ion. It is presumed that aqSOA particles contain a small amount of methyl-diimide. the mass spectrum also contains a fragmentation peak at  $m/z = 44$ . Alfarra et al. [51] suggested that the mass peak at  $m/z$  44 may be  $\text{COO}^+$  ion-generated by the cleavage of carboxylic acid compounds. This indicates that the aqSOA particles contain few carboxylic acid components.

Based on the main products of imidazoles that are obtained from the reaction of pyruvaldehyde with different concentrations of  $(\text{NH}_4)_2\text{SO}_4$ , and the information of hydrated products, methyl-diimine and carboxylic acids that are speculated from the mass spectrum of aqSOA particles (refer to the reaction mechanism of glyoxal and  $(\text{NH}_4)_2\text{SO}_4$  that was suggested by Lee et al. [23] and Maxut et al. [24]), the possible formation path of imidazoles that are formed from the aqueous reaction of pyruvaldehyde and  $(\text{NH}_4)_2\text{SO}_4$  is proposed in Figure 9.  $\text{NH}_4^+$  ion nucleophilically attacks the carbonyl oxygen atom of pyruvaldehyde to form the methyl-diimine intermediate (1). In addition,  $\text{NH}_4^+$  ion can catalyze the hydration of pyruvaldehyde to produce tetraol product (2). The H atom that is attached to the N atom on the diimine (1) undergoes the dehydration reaction with the OH

group on the tetraol product (2) to form an unstable intermediate (3). The lone pair electron nucleophilic of the N atom attacks the carbon atom in intermediate (3) and produces a positively charged intermediate (4) after dehydration. Intermediate (4) can undergo electron rearrangement and C–C cleavage to form 4-methyl-imidazole (6) and acetic acid. In addition, intermediate (4) can also form compound (7) through electron rearrangement, and (7) can be de-methanolized to yield 4-methyl-imidazole-2-carbaldehyde (8). Therefore, 4-methyl-imidazole and 4-methyl-imidazole-2-carbaldehyde are mainly produced in the aqueous reaction of pyruvaldehyde and  $(\text{NH}_4)_2\text{SO}_4$ .

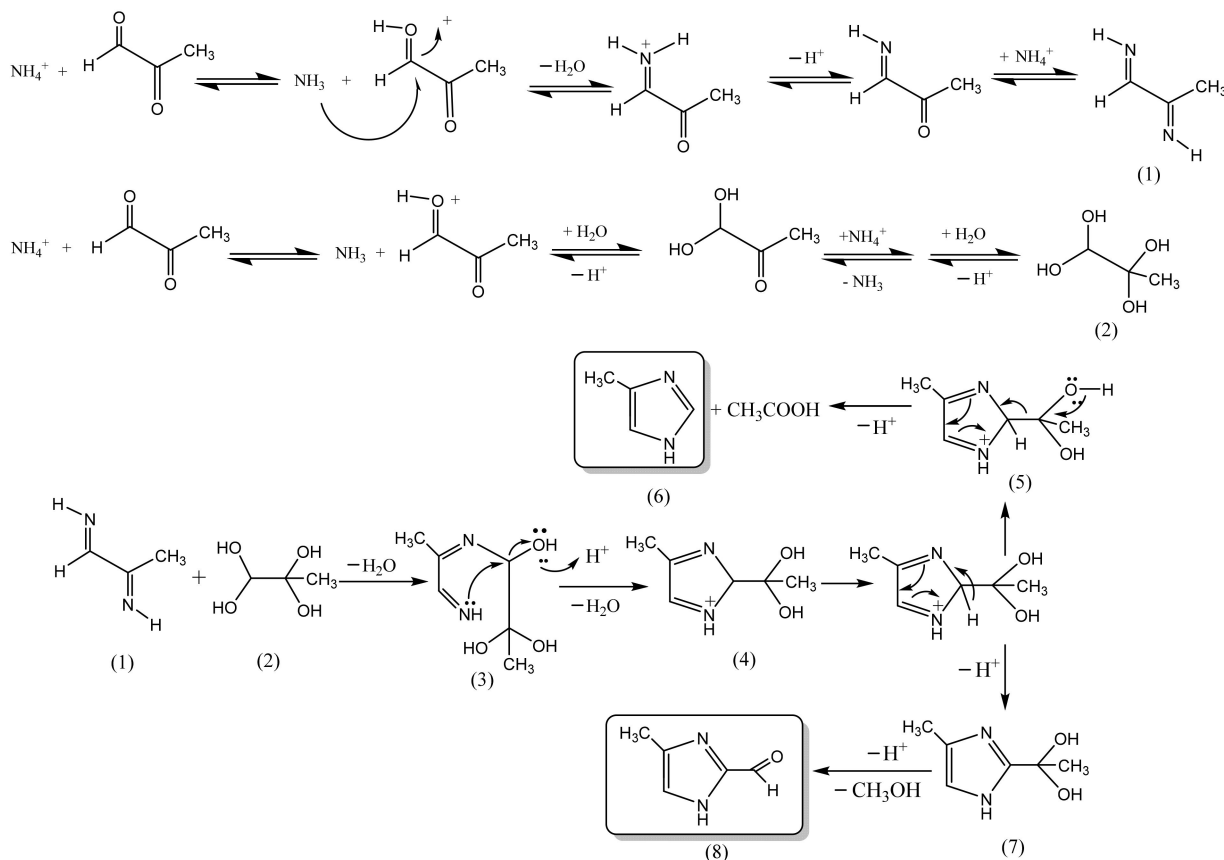


**Figure 9.** The possible formation path of imidazole products produced by the reaction of pyruvaldehyde and  $(\text{NH}_4)_2\text{SO}_4$ .

### 3.4. The Effect of Water-Soluble Anions on the MAC of aqSOA Particles

As the atmospheric aqueous phase contains different water-soluble anions, such as  $\text{CO}_3^{2-}$ ,  $\text{F}^-$ ,  $\text{NO}_3^-$ ,  $\text{SO}_4^{2-}$  and  $\text{Cl}^-$ , they can affect the activity of the  $\text{NH}_4^+$  ion and thus affect the optical properties of aqueous SOA particles. Therefore, the effects of water-soluble anions on the MAC of aqSOA produced by the reaction of pyruvaldehyde and ammonium ions are investigated in this study. A total of 5 mmol/L of pyruvaldehyde and 20 mmol/L of ammonium ions (10 mmol/L of  $(\text{NH}_4)_2\text{SO}_4$  and  $(\text{NH}_4)_2\text{CO}_3$ ; 20 mmol/L of  $\text{NH}_4\text{F}$ ,  $\text{NH}_4\text{NO}_3$  and  $\text{NH}_4\text{Cl}$ ) mixed solution is prepared and transferred to TSI 9302, atomized and dried to obtain aqSOA particles, successively. The extraction solutions of the aqSOA particles are shown in Figure 10. The extraction solution that is produced by pyruvaldehyde is colorless and transparent; the extraction solution that is formed from the aqueous reaction of pyruvaldehyde and  $\text{NH}_4\text{Cl}$ ,  $(\text{NH}_4)_2\text{SO}_4$  and  $\text{NH}_4\text{NO}_3$  is beige; and the extraction solution that is produced by the aqueous reaction of pyruvaldehyde,  $(\text{NH}_4)_2\text{CO}_3$  and  $\text{NH}_4\text{F}$  is brownish yellow and dark brown, respectively.

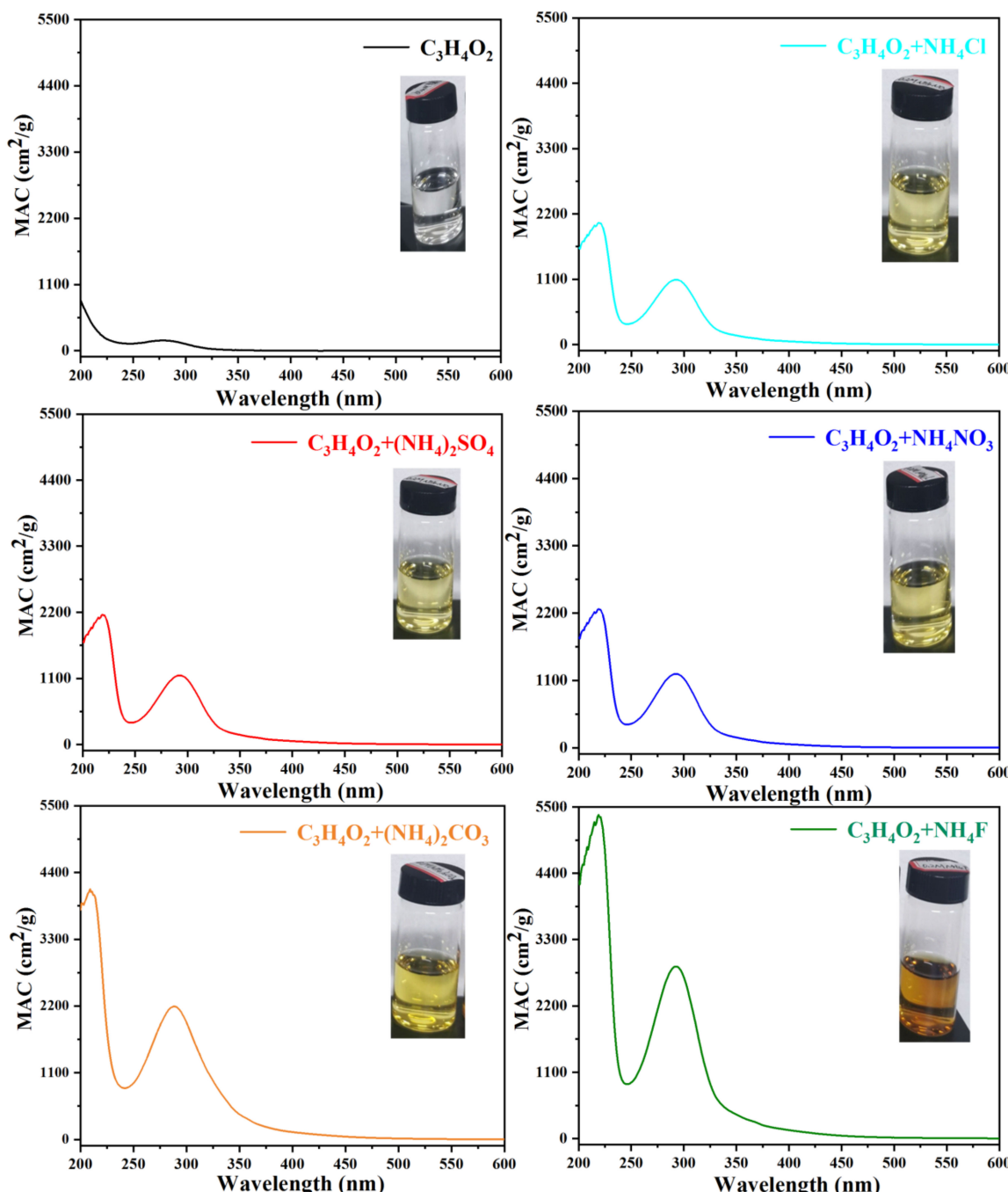


**Figure 10.** The MAC of the extraction solution of aqSOA particles produced by the mixed solution of 5 mmol/L pyruvaldehyde and 20 mmol/L ammonium ions.

Upon combining the total concentration of the organic carbon of 2% methanol in a water and extraction solution that is detected by the organic carbon analyzer, the  $C_{mass}$  of the extraction solution that is formed from the reaction of pyruvaldehyde and inorganic ammonium is listed in Table 1. According to the absorbance ( $A^{solution}$ ) in the UV-Vis absorption spectrum and the  $C_{mass}$  of the extraction solution of aqSOA particles, the calculated MAC values at 217 nm and 282 nm are displayed in Table 1, while the MAC of each extraction solution in 200–600 nm is shown in Figure 10. The extraction solution that is produced by pyruvaldehyde has a negligible absorbance in the range of 200–600 nm, consistent with its white color. The MAC of the aqSOA particles that are formed from the reaction of pyruvaldehyde and inorganic ammonium in the range of 200–600 nm is consistent with the absorption spectra that was detected by

Powelson et al. [28], Harrison et al. [30] and Aiona et al. [38]. The extraction solution has light absorption in the ultraviolet-near visible band with strong characteristic absorption at 217 nm and 282 nm, but almost no absorption at other wavelengths, showing that the absorption is wavelength-dependent [1]. This indicates that the extraction solution contains a brown carbon component of imidazole compounds. The MAC values of the aqSOA particles at 217 nm and 282 nm range from 1092 to 5340  $\text{cm}^2/\text{g}$ , which is about two orders of magnitude smaller compared to  $\text{MAC} = 5 \times 10^4 - 10^5 \text{ cm}^2/\text{g}$  for particles containing black carbon [52], but is comparable to the MAC of the brown carbon of field samples ( $1 \times 10^3 - 4 \times 10^4 \text{ cm}^2/\text{g}$ ) [1], and the MAC of brown carbon that is generated from the reaction of glyoxal and other carbonyl compounds with  $(\text{NH}_4)_2\text{SO}_4$  or amines ( $10^3 - 10^4 \text{ cm}^2/\text{g}$ ) [28]. It should be noted that the MAC of the aqSOA particles formed from the reaction of pyruvaldehyde and  $(\text{NH}_4)_2\text{SO}_4$  at 282 nm is 1146  $\text{cm}^2/\text{g}$ , slightly less than that of the MAC value (1330  $\text{cm}^2/\text{g}$ ) of brown carbon that is produced by methylglyoxal and  $(\text{NH}_4)_2\text{SO}_4$  reported by Harrison et al. [30]. Corresponding to the color of the extraction solution, the MAC of the extraction solution that is produced by the  $\text{C}_3\text{H}_4\text{O}_2 + \text{NH}_4\text{Cl}$ ,  $\text{C}_3\text{H}_4\text{O}_2 + (\text{NH}_4)_2\text{SO}_4$  and  $\text{C}_3\text{H}_4\text{O}_2 + \text{NH}_4\text{NO}_3$  aqueous reaction is low at 217 nm and 282 nm, while the MAC of the extraction solution that is formed from the  $\text{C}_3\text{H}_4\text{O}_2 + (\text{NH}_4)_2\text{CO}_3$  and  $\text{C}_3\text{H}_4\text{O}_2 + \text{NH}_4\text{F}$  aqueous reaction is relatively high, and the latter reaches the maximum value of 5340 and 2866  $\text{cm}^2/\text{g}$ , respectively.

**Table 1.** The total concentration of organic carbon,  $C_{mass}$ , MAC at 217 nm and 282 nm of extraction solution of aqSOA particles formed from the reaction of pyruvaldehyde and inorganic ammonium.

No	Extraction Solution	Total Concentration of Organic Carbon ( $\text{g}/\text{cm}^3$ )	$C_{mass}$ ( $\text{g}/\text{cm}^3$ )	217 nm MAC ( $\text{cm}^2/\text{g}$ )	282 nm MAC ( $\text{cm}^2/\text{g}$ )
1	2% methanol in water	0.00593	-	-	-
1	$\text{C}_3\text{H}_4\text{O}_2$	0.00714	0.00121	-	-
2	$\text{C}_3\text{H}_4\text{O}_2 + \text{NH}_4\text{Cl}$	0.00831	0.00238	2045	1092
3	$\text{C}_3\text{H}_4\text{O}_2 + (\text{NH}_4)_2\text{SO}_4$	0.00835	0.00242	2142	1146
4	$\text{C}_3\text{H}_4\text{O}_2 + \text{NH}_4\text{NO}_3$	0.00856	0.00263	2251	1173
5	$\text{C}_3\text{H}_4\text{O}_2 + (\text{NH}_4)_2\text{CO}_3$	0.00868	0.00275	4115	2185
6	$\text{C}_3\text{H}_4\text{O}_2 + \text{NH}_4\text{F}$	0.00875	0.00284	5340	2866

The  $\langle\text{MAC}\rangle$  of the extraction solution that averaged over 200–600 nm is obtained on the basis of Equations (1) and (2). As illustrated in Figure 11, the  $\langle\text{MAC}\rangle$  of the particulate matter extraction of pyruvaldehyde is the lowest at only 62.1  $\text{cm}^2/\text{g}$ . After adding inorganic ammonium salt, pyruvaldehyde reacts with inorganic ammonium to produce imidazoles with light-absorbing ability, and the  $\langle\text{MAC}\rangle$  value increases. The  $\langle\text{MAC}\rangle$  of the extraction solution that is produced by the  $\text{C}_3\text{H}_4\text{O}_2 + \text{NH}_4\text{Cl}$ ,  $\text{C}_3\text{H}_4\text{O}_2 + (\text{NH}_4)_2\text{SO}_4$  and  $\text{C}_3\text{H}_4\text{O}_2 + \text{NH}_4\text{NO}_3$  aqueous reaction increases to 138.6 and 140.2, and 144  $\text{cm}^2/\text{g}$ , successively. The  $\langle\text{MAC}\rangle$  of the extraction solution that is formed from the  $\text{C}_3\text{H}_4\text{O}_2 + (\text{NH}_4)_2\text{CO}_3$  and  $\text{C}_3\text{H}_4\text{O}_2 + \text{NH}_4\text{F}$  aqueous reaction is higher, raising to 243.9 and 324.9  $\text{cm}^2/\text{g}$ , respectively. The measured  $\langle\text{MAC}\rangle$  of the aqSOA that is generated by the reaction of pyruvaldehyde and inorganic ammonium is close to the value of the brown carbon that is produced by the ammonia aging of SOA (100–1000  $\text{cm}^2/\text{g}$ ) measured by Updyke et al. [43]. The  $\langle\text{MAC}\rangle$  of the extraction solution that is produced by the  $\text{C}_3\text{H}_4\text{O}_2 + \text{NH}_4\text{F}$  aqueous reaction is the highest, which contains the largest content of imidazole compounds. The  $\langle\text{MAC}\rangle$  of the extraction solution that is formed from the  $\text{C}_3\text{H}_4\text{O}_2 + \text{NH}_4\text{Cl}$  aqueous reaction is the lowest. The order of imidazole products generated by the reaction of pyruvaldehyde and ammonium ions that are promoted by inorganic anions is:  $\text{F}^- > \text{CO}_3^{2-} > \text{SO}_4^{2-} \approx \text{NO}_3^- \approx \text{Cl}^-$ .

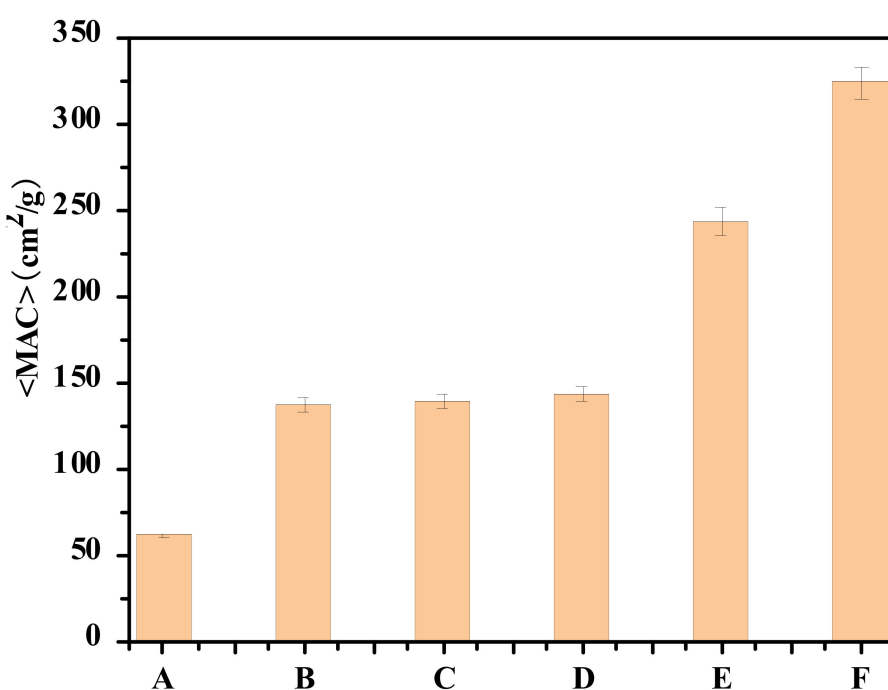


**Figure 11.** The  $\langle \text{MAC} \rangle$  averaged over 200–600 nm of extraction solution of aqSOA particles produced by the mixed solution of 5 mmol/L pyruvaldehyde and 20 mmol/L ammonium ions. (A— $\text{C}_3\text{H}_4\text{O}_2$ ; B— $\text{C}_3\text{H}_4\text{O}_2 + \text{NH}_4\text{Cl}$ ; C— $\text{C}_3\text{H}_4\text{O}_2 + (\text{NH}_4)_2\text{SO}_4$ ; D— $\text{C}_3\text{H}_4\text{O}_2 + \text{NH}_4\text{NO}_3$ ; E— $\text{C}_3\text{H}_4\text{O}_2 + (\text{NH}_4)_2\text{CO}_3$ ; F— $\text{C}_3\text{H}_4\text{O}_2 + \text{NH}_4\text{F}$ ).

According to the reaction mechanism for the formation of imidazoles shown in Figure 9, it can be known that the production of diimine and tetraol intermediates by ammonium ion and pyruvaldehyde is a prerequisite for the generation of imidazoles. Since the production of intermediates is accompanied by the generation of hydrogen ions, the formation of imidazoles is favorable under basic conditions.  $\text{NH}_4\text{Cl}$ ,  $\text{NH}_4\text{NO}_3$  and  $(\text{NH}_4)_2\text{SO}_4$  are strong acid ammonium salts and their solution is neutral, while  $(\text{NH}_4)_2\text{CO}_3$  and  $\text{NH}_4\text{F}$  are weak acid ammonium salts and their solutions are alkaline. The  $\text{pK}_b$  of  $\text{F}^-$  ion is 10.86, while the  $\text{pK}_{b1}$  and  $\text{pK}_{b2}$  of  $\text{CO}_3^{2-}$  is 3.75 and 7.62, respectively. The  $\text{pK}_b$  value of  $\text{F}^-$  ion is greater than that of  $\text{CO}_3^{2-}$ , so, under the conditions of the same volume and concentration, the alkaline of the  $\text{NH}_4\text{F}$  solution is greater than that of the  $(\text{NH}_4)_2\text{CO}_3$  solution [53]. In addition, in alkaline solution, it is conducive to the formation of ammonia. One hydrogen atom occupies the lone pair electrons on the nitrogen atom, reducing the affinity of ammonium ion. Ammonia that is formed by losing the hydrogen ion strengthens the nucleophilic attack ability, which is conducive to the reaction with pyruvaldehyde to produce diimine intermediate products [21,22]. Therefore, the  $\text{NH}_4\text{F}$  solution is most favorable for the generation of imidazole products, and the  $\langle \text{MAC} \rangle$  of the extraction solution that is produced by its reaction with pyruvaldehyde is the largest. The pH value order of the five inorganic ammonium salt solutions with the same concentration is:  $\text{NH}_4\text{F} > (\text{NH}_4)_2\text{CO}_3 > (\text{NH}_4)_2\text{SO}_4 \approx \text{NH}_4\text{NO}_3 \approx \text{NH}_4\text{Cl}$ . According to the above analysis, the order in which inorganic anions promote the reaction of pyruvaldehyde and ammonium ions to produce imidazole products is:  $\text{F}^- > \text{CO}_3^{2-} > \text{SO}_4^{2-} \approx \text{NO}_3^- \approx \text{Cl}^-$ .

Compared to the experiments of previous studies [21–24], our study simulates the atmospheric aqueous processing of pyruvaldehyde and ammonium ions to generate aqSOA particles via water evaporation, and the imidazoles in aqSOA are characterized using ALTOFMS in real-time and verified by off-line optical spectrometry. 4-methyl-imidazole and 4-methyl-imidazole-2-carbaldehyde are confirmed to be the main brown carbon products of the reaction between pyruvaldehyde and ammonium ions via the comprehensive analysis of the measured on-line mass spectrum and off-line absorption spectrum. Based on the laser desorption/ionization technology of ALTOFMS, the ion mass peak of the parent

molecule ( $M^+$ ), the characteristic cracking peaks and the structure information of organic compound can be obtained quickly, which can overcome the disadvantages of off-line analysis methods, such as cumbersome sample preparation and detection procedures. The ALTOFMS measurement results demonstrated that water evaporation accelerates the formation of imidazoles inside the droplets of pyruvaldehyde and ammonium ion.  $F^-$ ,  $CO_3^{2-}$ ,  $NO_3^-$ ,  $SO_4^{2-}$  and  $Cl^-$  ion aqueous phase can lead to the increase in content of imidazole compounds and enhanced light absorption capacity of aqSOA with the order of  $F^- > CO_3^{2-} > SO_4^{2-} \approx NO_3^- \approx Cl^-$ , as inorganic ammonium has a strong hygroscopic ability which can strengthen carbonyls partition into aqueous aerosol particles [54,55]. SOA that is generated from the water evaporation of aqueous aerosol containing high concentrations of inorganic ammonium may contribute to climate forcing.

#### 4. Conclusions

Imidazole compounds are important brown carbon components in atmospheric aerosol particles which play a vital role in climate radiative forcing. Pyruvaldehyde, ammonium sulfate and other inorganic ammonium salts are selected as the research objects, and aqSOA particles are generated by a home-made device in this study. The on-line measurement of ALTOFMS and off-line characterization of UV-Vis and ATR-FTIR demonstrate that 4-methyl-imidazole and 4-methyl-imidazole-2-carbaldehyde are the main components of aqSOA generated by the reaction of pyruvaldehyde and  $(NH_4)_2SO_4$ . By comparing the laser desorption/ionization mass spectra and the absorption spectra of the extraction of aqSOA particles, it can be concluded that water evaporation accelerates the formation of imidazoles inside the droplets, possibly owing to the highly concentrated environment.  $F^-$ ,  $CO_3^{2-}$ ,  $NO_3^-$ ,  $SO_4^{2-}$  and  $Cl^-$  can lead to the increase in the averaged mass absorption coefficient  $< MAC >$  in the range of 200–600 nm of aqSOA with the order of  $F^- > CO_3^{2-} > SO_4^{2-} \approx NO_3^- \approx Cl^-$ . These experimental results help to understand of the formation process of imidazoles via the aqueous chemistry of carbonyls and inorganic ammonium. However, the separation and quantitative research on the imidazole products are not carried out. The main focus of this study is the off-line measurement of  $< MAC >$ ; the study does not involve the on-line measurement of the extinction and scattering coefficient. In the subsequent experimental research, the high-performance liquid chromatography-mass spectrometry with a suitable chromatographic column can be considered to separate and quantitatively analyze the reaction products. In addition, the aerosol single-scattering albedometer can be used to detect the above parameters on-line to improve the optical properties of aqSOA particles.

**Author Contributions:** Conceptualization, M.H. and W.Z. (Wei jun Zhang); methodology, W.Z. (Wei jun Zhang) and X.G.; software, X.G. and C.H.; validation, M.H. and W.Z. (Wei jun Zhang); formal analysis, W.Z. (Weixiong Zhao); data curation, X.L.; writing—original draft preparation, X.L. and T.L.; writing—review and editing, M.H.; project administration, M.H.; funding acquisition, M.H. All authors have read and agreed to the published version of the manuscript.

**Funding:** This work is supported by the National Natural Science Foundation of China (No. 41575118), the Key Project of the Natural Science Foundation of Fujian Province, China (No .2020J02044) and the Natural Science Foundation of Fujian Province, China (No. 2021J01987). The authors thank Michael Nusbaum from the Department of English, Xiamen University, Tan Kah Kee College for language edits. The authors also express our gratitude to the referees for their valuable comments.

**Institutional Review Board Statement:** Not applicable.

**Informed Consent Statement:** Not applicable.

**Data Availability Statement:** Not applicable.

**Conflicts of Interest:** The authors declare no conflict of interest.

## References

1. Laskin, A.; Laskin, J.; Nizkorodov, S.A. Chemistry of atmospheric brown carbon. *Chem. Rev.* **2015**, *115*, 4335–4382. [[CrossRef](#)] [[PubMed](#)]
2. Hems, R.F.; Schnitzler, E.G.; Liu-Kang, C.; Cappa, C.D.; Abbatt, J.P.D. Aging of atmospheric brown carbon aerosol. *ACS Earth Space Chem.* **2021**, *5*, 722–748. [[CrossRef](#)]
3. Jo, D.S.; Park, R.J.; Lee, S.; Kim, S.W.; Zhang, X.A. Global simulation of brown carbon: Implications for photochemistry and direct radiative effect. *Atmos. Chem. Phys.* **2016**, *16*, 3413–3432. [[CrossRef](#)]
4. Kasthuriarachchi, N.Y.; Rivellini, L.H.; Adam, M.G.; Lee, A.K.Y. Light absorbing properties of primary and secondary brown carbon in a tropical urban environment. *Environ. Sci. Technol.* **2020**, *54*, 10808–10819. [[CrossRef](#)] [[PubMed](#)]
5. Evjen, S.; Høgmoen Åstrand, O.A.; Gaarder, M.; Paulsen, R.E.; Fiksdahl, A.; Knuutila, H.K. Degradative behavior and toxicity of alkylated imidazoles. *Ind. Eng. Chem. Res.* **2020**, *59*, 587–595. [[CrossRef](#)]
6. Ackendorf, J.M.; Ippolito, M.G.; Galloway, M.M. pH Dependence of the imidazole-2-carboxaldehyde hydration equilibrium: Implications for atmospheric light absorbance. *Environ. Sci. Technol. Lett.* **2017**, *4*, 551–555. [[CrossRef](#)]
7. Zhang, R.F.; Gen, M.S.; Liang, Z.C.; Li, Y.J.; Chan, C.K. Photochemical reactions of glyoxal during particulate ammonium nitrate photolysis: Brown carbon formation, enhanced glyoxal decay, and organic phase formation. *Environ. Sci. Technol.* **2022**, *56*, 1605–1614. [[CrossRef](#)]
8. Tinel, L.; Dumas, S.; George, C. A time-resolved study of the multiphase chemistry of excited carbonyls: Imidazole-2-carboxaldehyde and halides. *Comptes Rendus Chimie* **2014**, *17*, 801–807. [[CrossRef](#)]
9. Felber, T.; Schaefer, T.; Herrmann, H. Five-membered heterocycles as potential photosensitizers in the tropospheric aqueous phase: Photophysical properties of imidazole-2-carboxaldehyde, 2-furaldehyde, and 2-acetyl furan. *J. Phys. Chem. A* **2020**, *124*, 10029–10039. [[CrossRef](#)]
10. González Palacios, L.; Corral Arroyo, P.; Aregahegn, K.Z.; Steimer, S.S.; Bartels-Rausch, T.; Nozieère, B.; George, C.; Ammann, M.; Volkamer, R. Heterogeneous photochemistry of imidazole-2-carboxaldehyde: HO<sub>2</sub> radical formation and aerosol growth. *Atmos. Chem. Phys.* **2016**, *16*, 11823–11836. [[CrossRef](#)]
11. Corral Arroyo, P.; Aellig, R.; Alpert, P.A.; Volkamer, R.; Ammann, M. Halogen activation and radical cycling initiated by imidazole-2-carboxaldehyde photochemistry. *Atmos. Chem. Phys.* **2019**, *19*, 10817–10828. [[CrossRef](#)]
12. Tsui, W.G.; Rao, Y.; Dai, H.L.; McNeill, V.F. Modeling photosensitized secondary organic aerosol formation in laboratory and ambient aerosols. *Environ. Sci. Technol.* **2017**, *51*, 7496–7501. [[CrossRef](#)] [[PubMed](#)]
13. Martins-Costa, M.T.C.; Anglada, J.M.; Francisco, J.S.; Ruiz-López, M.F. Photosensitization mechanisms at the air–water interface of aqueous aerosols. *Chem. Sci.* **2022**, *13*, 2624–2631. [[CrossRef](#)] [[PubMed](#)]
14. Zarzana, K.J.; Min, K.E.; Washenfelder, R.A.; Kaiser, J.; Krawiec-Thayer, M.; Peischl, J.; Neuman, J.A.; Nowak, J.B.; Wagner, N.L.; Dubè, W.P.; et al. Emissions of glyoxal and other carbonyl compounds from agricultural biomass burning plumes sampled by aircraft. *Environ. Sci. Technol.* **2017**, *51*, 11761–11770. [[CrossRef](#)]
15. Ying, Q.; Li, J.Y.; Kota, S.H. Significant contributions of isoprene to summertime secondary organic aerosol in eastern United States. *Environ. Sci. Technol.* **2015**, *49*, 7834–7842. [[CrossRef](#)]
16. Volkamer, R.; Platt, U.; Wirtz, K. Primary and secondary glyoxal formation from aromatics: Experimental evidence for the bicycloalkyl–radical pathway from benzene, toluene, and p-xylene. *J. Phys. Chem. A* **2001**, *105*, 7865–7874. [[CrossRef](#)]
17. Qiu, X.H.; Wang, S.X.; Ying, Q.; Duan, L.; Xing, J.; Cao, J.Y.; Wu, D.; Li, X.X.; Xing, C.Z.; Yan, X.; et al. Importance of wintertime anthropogenic glyoxal and methylglyoxal emissions in Beijing and implications for secondary organic aerosol formation in megacities. *Environ. Sci. Technol.* **2020**, *54*, 11809–11817. [[CrossRef](#)]
18. Mitsuishi, K.; Iwasaki, M.; Takeuchi, M.; Okochi, H.; Kato, S.; Ohira, S.I.; Toda, K. Diurnal variations in partitioning of atmospheric glyoxal and methylglyoxal between gas and particles at the ground level and in the free troposphere. *ACS Earth Space Chem.* **2018**, *2*, 915–924. [[CrossRef](#)]
19. Fu, T.M.; Jacob, D.J.; Wittrocl, F.; Burrows, J.P.; Vrekoussis, M.; Henze, D.K. Global budgets of atmospheric glyoxal and methylglyoxal, and implications for formation of secondary organic aerosols. *J. Geophys. Res.* **2008**, *113*, 1–17. [[CrossRef](#)]
20. Herckes, P.; Valsaraj, T.; Collett, J.L., Jr. A review of observations of organic matter in fogs and clouds: Origin, processing and fate. *Atmos. Res.* **2013**, *132*, 434–449. [[CrossRef](#)]
21. Nozière, B.; Dziedzic, P.; Córdova, A. Products and kinetics of the liquid-phase reaction of glyoxal catalyzed by ammonium ions (NH<sub>4</sub><sup>+</sup>). *J. Phys. Chem. A* **2009**, *113*, 231–237. [[CrossRef](#)] [[PubMed](#)]
22. Kampf, C.J.; Jakob, R.; Hoffmann, T. Identification and characterization of aging products in the glyoxal/ammonium sulfate system—implications for light-absorbing material in atmospheric aerosols. *Atmos. Chem. Phys.* **2012**, *12*, 6323–6333. [[CrossRef](#)]
23. Lee, A.K.Y.; Zhao, R.; Li, R.; Liggio, J.; Li, S.M.; Abbatt, P.D. Formation of light absorbing organo-nitrogen species from evaporation of droplets containing glyoxal and ammonium sulfate. *Environ. Sci. Technol.* **2013**, *47*, 12819–12826. [[CrossRef](#)] [[PubMed](#)]
24. Maxut, A.; Nozière, B.; Fenet, B.; Mechakra, H. Formation mechanism and yield of small imidazoles from reactions of glyoxal with NH<sub>4</sub><sup>+</sup> in water at neutral pH. *Phys. Chem. Chem. Phys.* **2015**, *17*, 20416–20424. [[CrossRef](#)] [[PubMed](#)]
25. Teich, M.; Pinxteren, D.; Kecorius, S.; Wang, Z.; Herrmann, H. First quantification of imidazoles in ambient aerosol particles: Potential photosensitizers, brown carbon constituents, and hazardous components. *Environ. Sci. Technol.* **2016**, *50*, 1166–1173. [[CrossRef](#)]

26. Teich, M.; Schmidtpott, M.; Pinxteren, D.; Chen, J.M.; Herrmann, H. Separation and quantification of imidazoles in atmospheric particles using LC–Orbitrap–MS. *J. Sep. Sci.* **2020**, *43*, 577–589. [[CrossRef](#)]
27. Lian, X.F.; Zhang, G.H.; Yang, Y.X.; Lin, Q.H.; Fu, Y.Z.; Jiang, F.; Peng, L.; Hu, X.D.; Chen, D.H.; Wang, X.M.; et al. Evidence for the formation of imidazole from carbonyls and reduced nitrogen species at the individual particle level in the ambient atmosphere. *Environ. Sci. Technol. Lett.* **2021**, *8*, 9–15. [[CrossRef](#)]
28. Powelson, M.H.; Espelien, B.M.; Hawkins, L.N.; Galloway, M.M.; De Haan, D.O. Brown carbon formation by aqueous-phase carbonyl compound reactions with amines and ammonium sulfate. *Environ. Sci. Technol.* **2014**, *48*, 985–993. [[CrossRef](#)]
29. Tang, M.J.; Alexander, J.M.; Kwon, D.; Estillore, A.D.; Laskina, O.; Young, M.A.; Kleiber, P.D.; Grassian, V.H. Optical and physicochemical properties of brown carbon aerosol: Light scattering, FTIR extinction spectroscopy, and hygroscopic growth. *J. Phys. Chem. A* **2016**, *120*, 4155–4166. [[CrossRef](#)]
30. Harrison, A.W.; Waterson, A.M.; De Bruyn, W.J. Spectroscopic and photochemical properties of secondary brown carbon from aqueous reactions of methylglyoxal. *ACS Earth Space Chem.* **2020**, *4*, 762–773. [[CrossRef](#)]
31. Tutsak, E.; Koçak, M. High time-resolved measurements of water-soluble sulfate, nitrate and ammonium in PM<sub>2.5</sub> and their precursor gases over the Eastern Mediterranean. *Sci. Total Environ.* **2019**, *672*, 212–226. [[CrossRef](#)] [[PubMed](#)]
32. Huy, D.H.; Thanh, L.T.; Hien, T.T.; Takenaka, N. Comparative study on water-soluble inorganic ions in PM<sub>2.5</sub> from two distinct climate regions and air quality. *J. Environ. Sci.* **2020**, *88*, 349–360. [[CrossRef](#)] [[PubMed](#)]
33. Acharja, P.; Ali, K.; Trivedi, D.K.; Safai, P.D.; Ghude, S.; Prabhakaran, T.; Rajeevan, M. Characterization of atmospheric trace gases and water soluble inorganic chemical ions of PM<sub>1</sub> and PM<sub>2.5</sub> at Indira Gandhi International Airport, New Delhi during 2017–18 winter. *Sci. Total Environ.* **2020**, *729*, 138800. [[CrossRef](#)] [[PubMed](#)]
34. Sun, Z.L.; Duan, F.K.; He, K.B.; Du, J.J.; Zhu, L.D. Sulfate–nitrate–ammonium as double salts in PM<sub>2.5</sub>: Direct observations and implications for haze events. *Sci. Total. Environ.* **2019**, *647*, 204–209. [[CrossRef](#)] [[PubMed](#)]
35. Zhang, Y.; Yang, L.G.; Bie, S.J.; Zhao, T.; Huang, Q.; Li, J.S.; Wang, P.C.; Wang, Y.M.; Wang, W.X. Chemical compositions and the impact of sea salt in atmospheric PM<sub>1</sub> and PM<sub>2.5</sub> in the coastal area. *Atmos. Res.* **2021**, *250*, 105323. [[CrossRef](#)]
36. Zeebe, R.E.; Tyrrell, T. History of carbonate ion concentration over the last 100 million years II: Revised calculations and new data. *Geochim. Cosmochim. Acta* **2019**, *257*, 373–392. [[CrossRef](#)]
37. Lee, A.K.Y.; Zhao, R.; Gao, S.S.; Abbatt, J.P.D. Aqueous phase OH oxidation of glyoxal: Application of a novel analytical approach employing aerosol mass spectrometry and complementary off-line techniques. *J. Phys. Chem. A* **2011**, *115*, 10517–10526. [[CrossRef](#)]
38. Aiona, P.K.; Lee, H.J.; Leslie, R.; Lin, P.; Laskin, A.; Laskin, J.; Nizkorodov, S.A. Photochemistry of products of the aqueous reaction of methylglyoxal with ammonium sulfate. *ACS Earth Space Chem.* **2017**, *1*, 522–532. [[CrossRef](#)]
39. Huang, M.Q.; Hao, L.Q.; Guo, X.Y.; Hu, C.J.; Gu, X.J.; Zhao, W.X.; Wang, Z.Y.; Fang, L.; Zhang, W.J. Characterization of secondary organic aerosol particles using aerosol laser time-of-flight mass spectrometer coupled with FCM clustering algorithm. *Atmos. Environ.* **2013**, *64*, 85–94. [[CrossRef](#)]
40. Huang, M.Q.; Xu, J.; Cai, S.Y.; Liu, X.Q.; Hu, C.J.; Gu, X.J.; Zhao, W.X.; Fang, L.; Zhang, W.J. Chemical analysis of particulate products of aged 1,3,5-trimethylbenzene secondary organic aerosol in the presence of ammonia. *Atmos. Pollut. Res.* **2018**, *9*, 146–155. [[CrossRef](#)]
41. Feng, Z.Z.; Huang, M.Q.; Cai, S.Y.; Xu, X.Z.; Yang, Z.L.; Zhao, W.X.; Hu, C.J.; Gu, X.J.; Zhang, W.J. Characterization of single scattering albedo and chemical components of aged toluene secondary organic aerosol. *Atmos. Pollut. Res.* **2019**, *10*, 1736–1744. [[CrossRef](#)]
42. Lu, T.T.; Huang, M.Q.; Zhao, W.X.; Hu, C.J.; Gu, X.J.; Zhang, W.J. Influence of ammonium sulfate seed particle on optics and compositions of toluene derived organic aerosol in photochemistry. *Atmosphere* **2020**, *11*, 961. [[CrossRef](#)]
43. Updyke, K.M.; Nguyen, T.B.; Nizkorodov, S.A. Formation of brown carbon via reactions of ammonia with secondary organic aerosols from biogenic and anthropogenic precursors. *Atmos. Environ.* **2012**, *63*, 22–31. [[CrossRef](#)]
44. Panetta, R.J.; Ibrahim, M.; Yves Gélinas, Y. Coupling a high-temperature catalytic oxidation total organic carbon analyzer to an isotope ratio mass spectrometer to measure natural-abundance  $\delta^{13}\text{C}$ -dissolved organic carbon in marine and freshwater samples. *Anal. Chem.* **2008**, *80*, 5232–5239. [[CrossRef](#)] [[PubMed](#)]
45. Zawadowicz, M.A.; Abdelmonem, A.; Mohr, C.; Saathoff, H.; Froyd, K.D.; Murphy, D.M.; Leisner, T.; Cziczo, D.J. Single-particle time-of-flight mass spectrometry utilizing a femtosecond desorption and ionization laser. *Anal. Chem.* **2015**, *87*, 12221–12229. [[CrossRef](#)] [[PubMed](#)]
46. Liu, Y.; Liggio, J.; Staebler, R.; Li, S.M. Reactive uptake of ammonia to secondary organic aerosols: Kinetics of organonitrogen formation. *Atmos. Chem. Phys.* **2015**, *15*, 13569–13584. [[CrossRef](#)]
47. Silva, P.J.; Prather, K.A. Interpretation of mass spectra from organic compounds in aerosol time-of-flight mass spectrometry. *Analy. Chem.* **2002**, *72*, 3553–3562. [[CrossRef](#)]
48. Baeza-Romero, M.T.; Gaie-Levrel, F.; Mahjoub, A.; L'opez-Arza, V.; Garcia, G.A.; Nahon, L. A smog chamber study coupling a photoionization aerosol electron/ion spectrometer to VUV synchrotron radiation: Organic and inorganic-organic mixed aerosol analysis. *Eur. Phys. J. D* **2016**, *70*, 154–164. [[CrossRef](#)]
49. Lemai, V.; Legaard, E.; Thrasher, C.; Jaffe, A.; Berden, G.; Martens, J.; Oomens, J.; O'Brien, R.E. UV/Vis and IRMPD spectroscopic analysis of the absorption properties of methylglyoxal brown carbon. *ACS Earth Space Chem.* **2021**, *5*, 910–919.
50. Huang, M.Q.; Xu, J.; Cai, S.Y.; Liu, X.Q.; Zhao, W.X.; Hu, C.J.; Gu, X.J.; Fang, L.; Zhang, W.J. Characterization of brown carbon constituents of benzene secondary organic aerosol aged with ammonia. *J. Atmos. Chem.* **2018**, *75*, 205–218. [[CrossRef](#)]

51. Alfarra, M.R.; Paulsen, D.; Gysel, M.; Garforth, A.A.; Dommen, J.; Prévôt, A.S.H.; Worsnop, D.R.; Baltensperger, U.; Coe, H. A mass spectrometric study of secondary organic aerosols formed from the photooxidation of anthropogenic and biogenic precursors in a reaction chamber. *Atmos. Chem. Phys.* **2006**, *6*, 5279–5293. [[CrossRef](#)]
52. Bond, T.; Bergstrom, R. Light absorption by carbonaceous particles: An investigative review. *Aerosol Sci. Technol.* **2006**, *40*, 27–67. [[CrossRef](#)]
53. Sanger, M.J.; Danner, M. Aqueous ammonia or ammonium hydroxide? Identifying a base as strong or weak. *J. Chem. Educ.* **2010**, *87*, 1213–1216. [[CrossRef](#)]
54. Kroll, J.H.; Ng, N.L.; Murphy, S.M.; Varutbangkul, V.; Flagan, R.C.; Seinfeld, J.H. Chamber studies of secondary organic aerosol growth by reactive uptake of simple carbonyl compounds. *J. Geophys. Res. Atmos.* **2005**, *110*, 1–10. [[CrossRef](#)]
55. Ip, H.S.S.; Huang, X.H.H.; Yu, J.Z. Effective Henry's law constants of glyoxal, glyoxylic acid, and glycolic acid. *Geophys. Res. Lett.* **2009**, *36*, L01802. [[CrossRef](#)]